Plasmon Coupled Fluorescence in Gold Nanorods for Enhanced Optical Detection of Oligonucleotides

Inês Isabel Resende e Silva*

** Instituto Superior Técnico, email: ines.resende.e.silva@ist.utl.pt*

The tips of gold nanorods (AuNRs) are hotspot regions with remarkable near field amplification of incident electromagnetic field, capable of enhancing the fluorescent emission of dyes in their vicinity. Molecular beacons are oligonucleotide sequences that emit a fluorescent signal when hybridization with target sequence occurs. The detection range of these probes is restricted by the intensity of the “on” fluorescent signal relatively to the “off” state. Therefore, the conjugation of AuNRs with selectively positioned molecular beacons is a promising strategy for the development of a nanohybrid sensor for enhanced optical detection of oligonucleotides. This work is integrated in the ongoing research for the development of said sensor, and gives a meaningful contribution through the characterization of fluorescence emission of the molecular beacons and DNA-AuNRs nanohybrids. First, fluorescence enhancement effects in AuNRs (25 x 71 nm) loaded with a ATTO647N-labelled dsDNA 10-bp spacer were characterized at single particle level through confocal fluorescence lifetime microscopy. Single particle study of DNA-AuNRs nanohybrids supported that indiscriminately loaded AuNRs required 10-fold more dye to reach fluorescence emission Tip-selective AuNRs. Then, molecular beacon probes bearing the organic quenchers DDQII and QSY21 were studied in the absence of AuNRs, in regard to their quantum yield and fluorescence lifetime by conventional spectroscopy. The molecular beacons showed negligible quantum yield increase in the presence of target sequence, leading to their exclusion, under the conditions studied, as suitable oligonucleotide recognition moieties for the in-development DNA-AuNRs nanobiosensors.

Keywords: Plasmon enhanced fluorescence, metal nanoparticles, single particle spectroscopy, fluorescence imaging

Molecular beacons are oligonucleotide sequences that form a stem-and-loop structure and are labelled with a quencher at one end and a fluorophore at the other, thus only emitting fluorescent signal when target sequences hybridize to the complementary loop sequence. The detection range of these sensors is restricted by the intensity of the “on” fluorescent signal relatively to the “off” state. Hence, the enhancement of fluorescence emission in the “on” state could raise the sensitivity of these sensors.

For fluorescence based optical sensing, gold nanoparticles (AuNPs) can act as antennas, amplifying the signal of neighbouring fluorescent molecules, through enhancement of the excitation rate and quantum yield [1]. This phenomenon, called plasmon enhanced fluorescence (PEF), depends crucially on the dye’s position at the particle’s surface and it can be particularly strong at specific surface regions, known as plasmon hotspots. Therefore, the conjugation of AuNPs with selectively positioned molecular beacons is a promising strategy for the development of a nanohybrid sensor for enhanced optical detection of oligonucleotides. The present work delves into the parts of one such nanostructure: AuNRs functionalized with dye-labelled alkanethiol-oligonucleotides (DNA-AuNRs).

In the proof-of-concept, a red emitting dye (ATTO647N) was 10-bp away from the AuNR surface, covalently labelled at the terminus of a dsDNA spacer, here termed BF1BT. The purpose of this research was to set the groundwork for the development of a high sensitivity PEF-based sensor towards target oligonucleotides, consisting of AuNRs decked with molecular beacons with specificity towards oligonucleotide biomarkers for medical

A

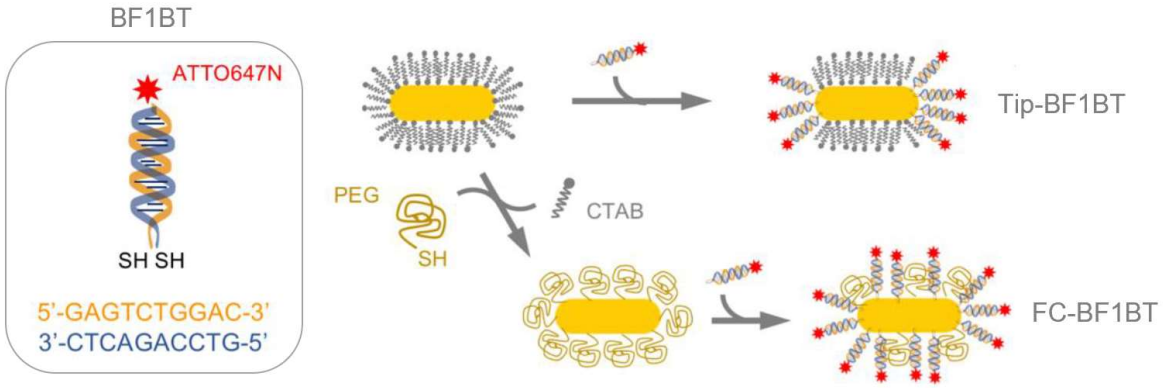

B

	strands/AuNR	F/F_0
Tip-1h	36	7.2
Tip-6h	93	3.7
FC-ON	327	0.8
FC400-1h	102	0.3

C

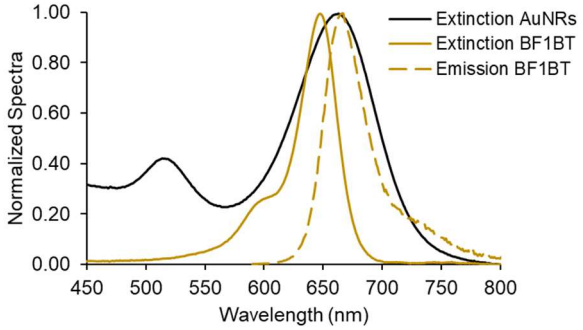

Figure 1: A Schematic of BF1BT and functionalization protocols for DNA-AuNRs. Top – Tip-selective process. Bottom – Fully-coated process. Adapted from [2]. B - Summary table of ME-quantification of BF1BT strands per AuNR and relative fluorescence enhancement at 600 nm excitation, identified according to variations in protocol: for FC, the loading ratio was either 400:1 for a functionalization time of 1 h or 4000:1 for an overnight (ON) functionalization. For tip, the loading ratio was always 4000:1, but the functionalization time was either 1 h or 6 h. C - Normalized extinction and emission spectra of BF1-BT in 1x PB- S and AuNRs in CTAB (10 mM).

diagnostics – examples were selected for the infection with dengue virus or sleeping sickness, and for circulatory miRNA-145.

The present work supports the ongoing research at host laboratory. First, the emission properties of dye-AuNR hybrids, as characterized by single-particle spectroscopy, are described and compared to previous results of ensemble emission spectroscopy to evaluate plasmon-coupled emission in these systems. Next, the functionality of DNA hairpin probes designed to perform fluorescence signalling of target oligonucleotide sequences is analysed from results of ensemble emission and fluorescence decay measurements. Finally, the conjugation of the DNA hairpin probes onto AuNR antennas to produce a nanohybrid biosensor and its response to target sequences were assessed by ensemble emission or confocal fluorescence microscopy.

CONTEXT FROM HOST LABORATORY

Plasmonic Enhanced Fluorescence and FRET in DNA-AuNRs

Previously at CQE8 group, two colloidal functionalization approaches were established to load alkanethiol dye-labelled oligonucleotides onto AuNRs: fully-coated (FC) through a PEG/Tween20 assisted ligand-exchange approach, and tip-selective (Tip) exploiting the CTAB bilayer that stabilizes AuNRs. Stationary state fluorometry showed that the fluorescence readout was considerably greater in Tip nanohybrids compared to free dye, due to the AuNRs' antenna effect. In FC nanohybrids, quenching of fluorescence was verified [2].

The absorption and emission spectra of free ATTO647N overlap with the plasmon longitudinal resonance band of the commercial AuNRs (25 x 71 nm), a necessary condition for maximization of fluorescence enhancement. Roughly, the absorption overlap allows for the

enhancement of local field on the excitation rate, taking the dye more frequently to the excited state whereas the overlap of the emission spectra contributes to the enhancement of the photophysical decay rates, due to the higher local density of states resulting from the nanoantenna effect. In this dye/NP pair, the amplification of the excitation rate is expected to be the main contributor for enhanced fluorescence.

The conjugation of fluorescently labelled DNA oligonucleotides onto AuNRs is sought as a preliminary study toward the development of nanobiosensors comprising DNA hairpin probes for the detection of nucleic acids.

The designed DNA probes have the same 10-bp spacer for optimal positioning of ATTO647N, but the equivalent to BT sequence was extended to comprise a loop region that ends with a quencher. The loop region has a sequence complementary to a specific target sequence. In the absence of target, the hairpin probe would be closed, ensuring quenching of ATTO647N, i.e. a state of high FRET, low emission, while hybridization with the target is expected to open the hairpin, thus resulting in a state of low FRET, high emission, that signals target recognition.

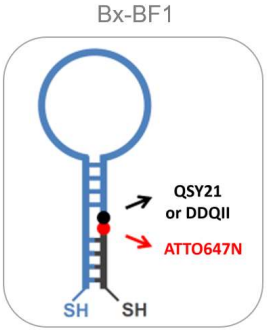

Figure 2: Molecular beacon design: quencher-labelled hairpin hybridizes at the stem with ATTO647N-labelled BF1.

The nanoantenna effect of AuNRs would contribute in two ways for the increased detection sensibility of this nanohybrids over conventional molecular beacons: 1) modulation FRET between donor ATTO647N and acceptor organic quencher, ensuring efficient fluorescence quenching in the closed hairpin; 2) fluorescent enhancement of ATTO647N in open hairpin.

EXPERIMENTAL SETTINGS

Chemicals and Materials: Ultrapure water was used for all experiments, obtained with a Milli-Q purification system (Merck-Millipore). Thiolated poly(ethylene glycol) (mPEG-SH, MW~5,000), poly(vinyl alcohol), Tween 20, CTAB (99%), sodium citrate tribasic dihydrate (99,5%) and citric acid (99,5%) were acquired from Sigma-Aldrich. PBS tablets were acquired from Sigma-Aldrich and ThermoFisher Scientific.

Colloidal AuNRs with 25 nm diameter, ca 71 nm in length, and plasmon peak at 650 nm (15% dispersion) were acquired from Nanopartz in CTAB aqueous suspension. ATTO647N was purchased from ATTO-TEC GmbH. Modified oligonucleotide sequences were purchased from STABVIDA, except BD2, BM2 and BS2 that were purchased from ThermoFisher Scientific. Sequences and modifications are explicitly described in Table 1.

Equipment: UV−vis extinction spectra were measured in a spectrophotometer from PerkinElmer, model Lambda 35. Corrected fluorescence emission spectra were acquired with a FluoroLog-3 spectrofluorimeter (Horiba Jobin Yvon). Cuvettes with a 10 mm light path and 700 μL capacity made of Quartz SUPRASIL (Hellma) were used for all experiments.

The CFLM used was a MicroTime 200 (PicoQuant GmbH). Details of set-up in [3]. For image acquisition, the excitation wavelength of the laser was 639 nm (LDH 635-b, PicoQuant) with a pulse repetition rate of 20 MHz. For single spectra acquisition, the excitation wavelength of the laser was 482 nm (LDH 485, PicoQuant) at 40 MHz and 50 kW/cm^2 irradiation with collection on a QE Pro (Ocean Optics) spectrometer.

METHODOLOGY

Protocols defined in [2]: *DNA-AuNRs Tip-Selective and Fully-Coated Functionalization; immobilization of PVA samples; Quantification of Alkanethiol-Oligonucleotides loaded on AuNRs and Calculation of Relative Fluorescence Enhancement.*

Immobilization of AuNRs: Drop casting was performed to adsorb functionalized Tip AuNRs onto MPTMS treated coverslips. Stock AuNRs were immobilized via spin-coating.

Table 1: ssDNA oligonucleotide sequences and respective modifications.

Label	Modifications	Nucleotide Sequence
BF1	5' ATTO647N 3' C6 Thiol	5'-GAG TCT GGA C-3'
BT	5' C6 Thiol	5'-GTC CAG ACT C-3'
DF1	5' Thioctic Acid 3' ATTO647N	5'-TGG TCG TTG AAG TCG AGG CCT GTT CTC GGA GAG CGA CCA-3'
BD1	5' C6 Thiol 3' DDQII	5'-GTC CAG ACT CCA AGT GGT CGT TGA AGT CGA GGC CTG TTC TCG GAG AGC GAC CA-3' Target: 5'-CUC UCC GAG AAC AGG CCU CGA CUU CAA-3'
BD2	5' C6 Thiol Modifier S-S 3' QSY21	
BM1	5' C6 Thiol 3' DDQII	5'-GTC CAG ACT CCA AGT GGT CGC AGG TCA AAA GGG TCC TTA GGG ACG ACC A-3' Target: 5'-UCC CUA AGG ACC CUU UUG ACC UG-3'
BM2	5' C6 Thiol Modifier S-S 3' QSY21	
BS2	5' C6 Thiol Modifier S-S 3' QSY21	5'-GTC CAG ACT CCA AGT GGT CGC AAG TGC GTA AAC ACA ACG ACC A-3' Target: 5'-TTG TGT TTA CGC ACT TG-3'

Relative Determination of Fluorescence Quantum Yield: The quantum yield was obtained through a relative determination method [4][5], with cresyl violet chosen as the standard dye and an excitation wavelength of 580 nm. Concentration of probe, BF1 and target was 1, 0.5 and 2 μM.

Fluorescence Decays Measurements: All samples were excited at 0.08 kW/cm^2 for 2 min.

MATLAB Routines for 3D Gaussian Fitting of Point Spread Function Single Particle Spectral Fitting: From SymPhoTime software (PicoQuant GmbH), intensity weighted FLIM images were extracted for visual sample comparison and the point spread function of each bright spot was fitted with a 3D Gaussian, through a MATLAB routine built off two existing contributions on the MathWorks - File Exchange entry: Image Segmentation Tutorial (version 1.6.0.0) by Image Analyst [6] and Fast Gaussian Point Spread Function Fitting (MEX) by Simon Christoph Stein [7]. The implemented routine builds a mask of regions of interest (ROI) and extracts peak intensity from the anisotropic 3D Gaussian fittings.

Single particle spectra were fitted with a Lorentzian function as established in literature for individual AuNRs [8][9].

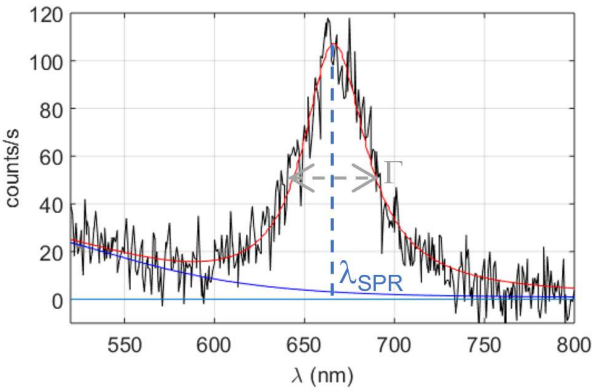

Figure 3: Example of the photoluminescence spectrum of a single rod and respective Lorentzian fitting to determine the peak wavelength λ_{SPR} (666 nm) and linewidth Γ (118 meV).

RESULTS AND DISCUSSION

Single Particle Fluorescence Spectroscopy of AuNRs-BF1BT

The immobilization of DNA-AuNRs made it possible to characterize and compare the emission of single particle structures according to the different functionalization and immobilization protocols.

CFLM intensity images for dye-labelled AuNRs were obtained at an excitation power of 0.04 kW/cm^2. At this excitation power, the strong brightness of each spot can be associated to the dye-NP coupled emission of BF1BT decorated AuNRs rather than NP scattering, since for the same conditions it is impossible to detect luminescence in non-labelled AuNRs, such as H_2O Stock samples (Figure 4B). CFLM intensity images for PVA samples (Figure 4C,D) were remarkably brighter than H_2O samples (Figure

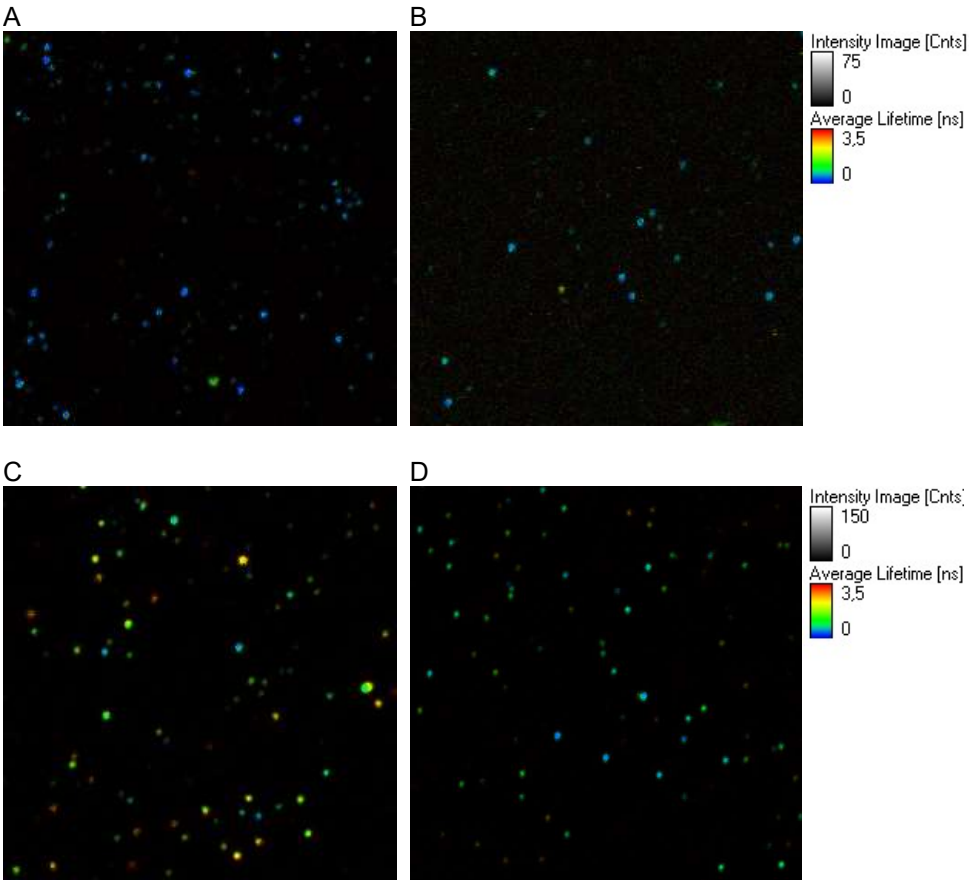

E

	Individual Fraction
H_2O Tip-1h	50%
H_2O Tip-6h	76%
H_2O STOCK	97%
PVA Tip-1h	61%
PVA Tip-6h	52%
PVA FC-ON	83%
PVA FC400-1h	81%
PVA LE	84%

Figure 4: CFLM 40 x 40 μm images at 639 nm laser irradiation. A – H_2O Tip-1h at 0.04 kW/cm^2; B - H_2O stock at 20 kW/cm^2; C – PVA Tip-1h at 0.04 kW/cm^2; D – PVA FC-ON at 0.04 kW/cm^2 ; E – Individual fraction – percentage of well-defined single AuNR recovered spectra for each sample.

4A). This might be a matter of geometrical optics, related to the higher refractive index of PVA (ca 1.45) relatively to water (ca 1.33).

The Lorentzian fitted photoluminescence spectrum allowed the extraction of resonance wavelength λ_{SPR} and the full width at half-maximum (FWHM) Γ of each AuNR and was used to assess the individual AuNR fraction per sample (Figure 4E).

The individual fraction is lowered in DNA-AuNRs by the presence of aggregates. It is most likely that this aggregation occurs at the fixation steps, because the extinction spectra of the same samples in colloidal dispersion do not show typical characteristics of aggregated samples, such as broadened spectra or strongly shifted peaks.

Looking into the resonance wavelength of each AuNR sample, the PVA FC samples displayed the longer λ_{SPR} (Figure 5A). Prima facie, this in accordance to previous works that have shown that the attachment of molecules to a AuNR induces a red-shift in the λ_{SPR}, which scales with the number of bonds [10]. However, the PVA Tip samples had a blue shift relative to stock samples. It was thus theorized that the main factor affecting λ_{SPR} in PVA samples was the refractive index. Possibly, in PVA FC samples, PEG covers the sides of the AuNR, ensuring a complete encapsulation of the particle, whereas in PVA Tip samples, the sides of the AuNR are exposed, resulting in a lower (closer to air) local refractive index.

Regarding the FWHM (Figure 5B), Γ has been shown to increase with AuNR width [11] and the adsorption of thiol molecules to the surface [10][12]. Across all samples, the effect of thiol adsorption as a broadener of linewidth is not apparent and once again the PVA Tip samples deviate with a Γ of 140 meV, relatively to ca. 120 meV of all other samples. This data is not coherent with previous work [13], in which AuNRs tip-selectively functionalized with biotin showed little broadening compared to fully-coated.

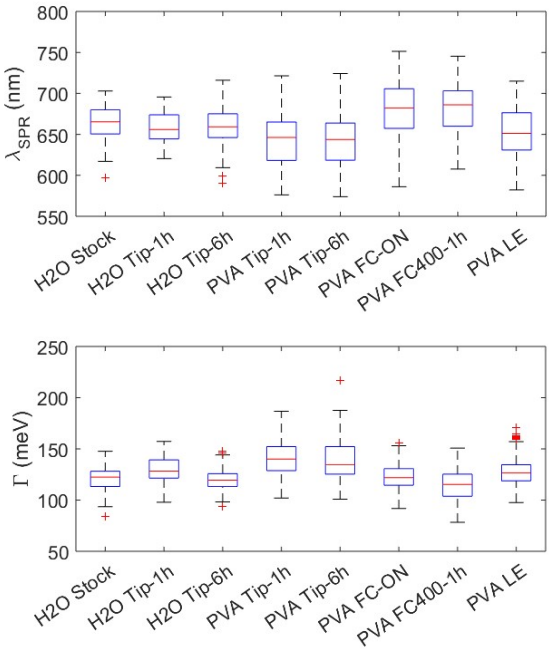

Figure 5: Boxplot of the surface plasmon resonance wavelength and FWHM obtained from Lorentzian fitting of single particle spectra.

After correlating the spectral data from the AuNRs' photoluminescence with the peak intensity data from Gaussian fitted bright spots, histograms of peak intensity exclusively of single AuNRs were built (Figure 6). Prima facie, the broad dispersion in peak intensity for all samples, mainly the Tip-1h, Tip-6h and FC-ON, supports the premise that the functionalization protocols yield samples with a significant dispersion in the actual number of chains per NP. Apparently, a great number of AuNRs contain a small amount of dyes, while a few are greatly loaded and are thus more fluorescent.

When one considers the number of chains of each sample, sample comparison appears to support that brightness is more dependent on the "correct" location of said chains, rather than its real amount, as expected from DDA simulations [2].

In FC400-1h (102 strands/AuNR), the overall brightness of the sample is considerably lower than that of Tip-6h (93 strands/AuNR) (Figure 32C,D). In the first sample, each AuNR is only sparsely decorated with DNA, decreasing the

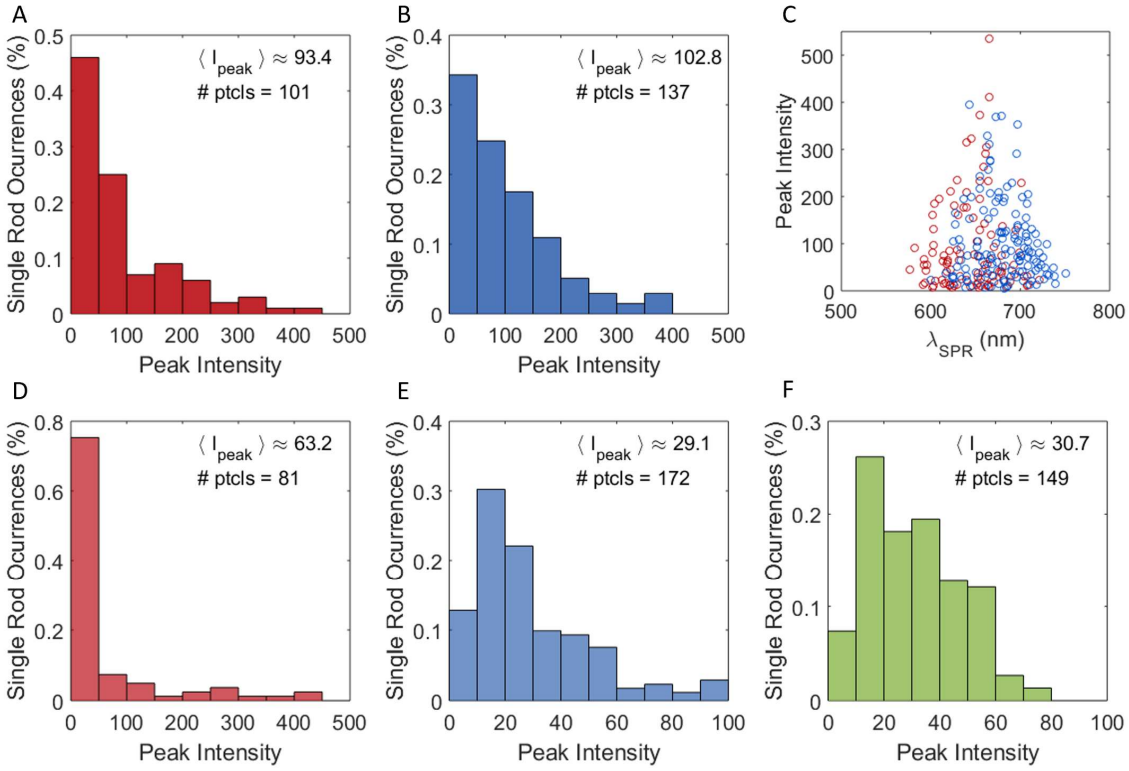

Figure 6: Histogram of Peak Intensity of single AuNRs in samples irradiated at 639 nm. Samples A – PVA Tip-1h; B – PVA FC-ON; C – PVA Tip-6h; D – PVA FC400-1h were irradiated at 0.04 kW/cm^2. E – PVA LE was irradiated at 4 kW/cm^2. F - Scatter graph of Peak Intensity relatively to surface plasmon resonance wavelength: PVA Tip-1h (o) and PVA FC-ON (o).

likelihood of DNA strands to insert themselves at the tip of the AuNRs.

When comparing the Tip-1h (36 strands/AuNR) and FC-ON (327 strands/AuNR), it becomes apparent that the higher dye loading does not translate in increased brightness. Furthermore, it can be conjectured that with the high number of dyes per NP in the FC sample, a significant amount of DNA strands will eventually end up attached at the tips of the AuNRs, leading to similar levels of brightness. Indeed, visual inspection of CFLM images of PVA Tip-1h and PVA FC-ON were already suggestive of this result, as there was no significant difference in brightness of both samples (Figure 4C,D).

This result was coherent with previously obtained ensemble measurements that supported the premise that tip-selective loading of dye-labelled DNA oligonucleotides onto AuNRs yields nanohybrids capable of superior dye emission enhancement.

Correlating peak intensity with λ_{SPR} for each AuNR in the PVA Tip-1h and FC-ON samples (Figure 6C), it was expected from previous simulation results that maximum brightness would be obtained for AuNRs with λ_{SPR}. around 650 nm. In fact, the higher values occur within the 650-680 nm range, which was in agreement with the simulation, but was weighted down by the significant number of AuNRs with plasmon at the same wavelength and non-remarkable brightness.

This mismatch between simulation and experimental data has its origins in the heterogeneity in the amount, location and orientation of dye per AuNR, due to the stochastic nature of the conjugation of DNA onto AuNRs [14][15].

Fluorescence Signalling in Molecular Beacons for Oligonucleotide Detection

The values of quantum yield obtained through the relative determination method for ATTO647N and BF1BT matched the known value for ATTO647N dye in aqueous solution. According to specification sheet, ATTO647N has a quantum yield of 65% [16] and a value of 62% was obtained for both species.

Fluorescence decays were performed in the CFLM setup for both samples and surprisingly, BF1BT required bi-exponential fitting exhibiting a minor (<10%) 1 ns component and a dominant 4.1 ns lifetime component, considerably longer than free dye (one component ~3.5 ns).

When quencher probes were added to BF1 in order to assemble the steam-loop molecular beacon as represented in Figure 2, the fluorescence quantum yield for the DDQII quencher based molecular beacons was of about 45% while for the QSY21 molecular beacons it was of about 10%. The high value of quantum yield for DDQII molecular beacons was evidence of ineffective quenching. Hence, once target was injected into the system, only a marginal increase in fluorescence output could be expected. For this reason, the next discussion will focus on the QSY21 molecular beacons.

To assess the target response potential of QSY21 molecular beacons, the quantum yield of these DNA hairpin probes was used to calculate transfer efficiency.

Table 2: Transfer efficiency for QSY21-ATTO647N from experimental quantum yield data.

	$\boldsymbol{\Phi_T = \frac{\Phi_F^{BF1BT} - \Phi_F^{x}}{\Phi_F^{BF1BT}}}$
BD2BF1	
w/o Target	76%
w/Target	73%
BM2BF1	
w/o Target	81%
w/Target	73%
BS2BF1	
w/o Target	84%
w/Target	81%

Assuming long-distance dipole-dipole interaction between dye and quenchers, a theoretical transfer efficiency curve (Figure 7) can be built after calculation of Förster's radius (R_0) from the normalized emission spectrum of ATTO647N and the absorption spectra of a quencher-labelled sequence. Comparing the theoretical efficiency curve (Figure 7) with the transfer efficiencies obtained through the fluorescence quantum yield Table 2, it is possible to estimate dye-quencher distance.

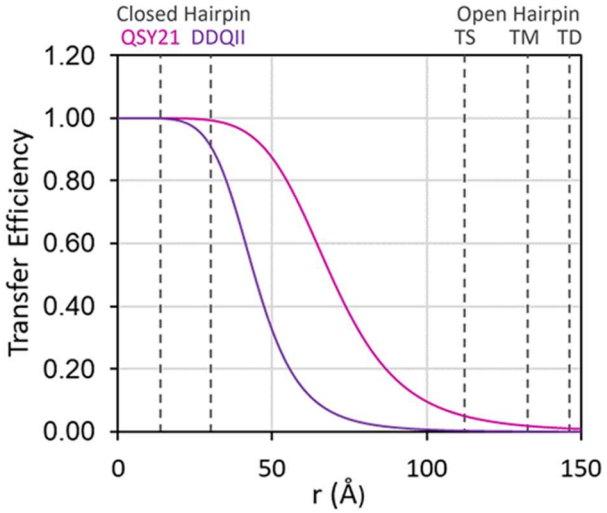

Figure 7: Transfer Efficiency of DDQII (purple) and QSY21 (pink) to ATTO647N.

For the BS2BF1 beacon in the absence of target, the obtained dye-quencher distance for a transfer efficiency of 84% is of about 52 Å. This value is below expectation for a well-assembled molecular beacon with a closed hairpin. Pondering approximate molecular lengths, the distance should be of the order of 14 Å for QSY21 (Figure 7).

The mismatch between the expected and the quantum yield calculated transfer efficiency might result from a combination of two factors: 1) the equilibrium constant for ssDNA-dsDNA association is such that at the molar ratios between probe sequence and BF1, not all dye-labelled strands are hybridized with quencher-labelled arm; 2) DNA hairpins may remain in the open conformation (low FRET, high emission).

Assuming that the second hypothesis has only a minor contribution, the obtained transfer efficiency for QSY21 molecular beacons can be considered acceptable for the OFF state, with the understanding that the process of loading molecular beacons onto the AuNRs might favour a well-assembled stem.

Upon hybridization with target (Table 2) a significant decrease in transfer efficiency would be expected. However, what was obtained was a variation in transfer efficiency for all molecular beacons of less than 10 %, which renders an increase of less than 10 Å in dye-quencher distance. Since the efficiency transfer decrease upon insertion of target was consistently low throughout all samples, it strongly suggests that the hairpin is not opening, likely due to secondary structures, which lower the association rate with target sequences.

Future work will need to focus on assessing the impact of salt concentration on the ON and OFF states of the designed molecular beacons, since excessive salt concentration has been reported to stabilize closed and secondary conformations to the detriment of an open hairpin [17].

Fluorescence Signalling of DNA-AuNRs biosensors in Response to Dengue Target

Preliminary work at host laboratory with molecular beacon FC DNA-AuNRs only showed partial response to target in suspension MCS traces.

Since there was an absence of significant sensor response, a simpler molecular beacon was designed, consisting of an ATTO647N labelled probe (DF1) against target dengue sequence. Contrary to previous probes, this one was lacking in the 10-bp spacer. Instead, in the closed hairpin conformation the fluorescence emission of ATTO647N would be quenched directly by the AuNR.

Two samples were tested for sensor performance in response to a dengue virus target: 1) FC-1h-DF1 (52 strands/AuNR), which had been previously assessed to have no response at room temperature, was thus subjected to heat shock to promote hairpin opening; 2) InSituDF1 was a surface-functionalized sample.

For the first sample, the heat shock protocol (90 ºC, 5 min) was applied with weak results to FC-1h-DF1 (Figure 8A) likely due to narrow readout range, resulting from low probe loading.

For the second sample, assessing target response at single particle level for InSituDF1 (Figure 8B), there was an increase in brightness of about 1.5-fold after approximately one-hour hybridization.

Nonetheless, on the whole, target response in the applied conditions for the AuNRs-DF1 systems showed little potential for sensor application.

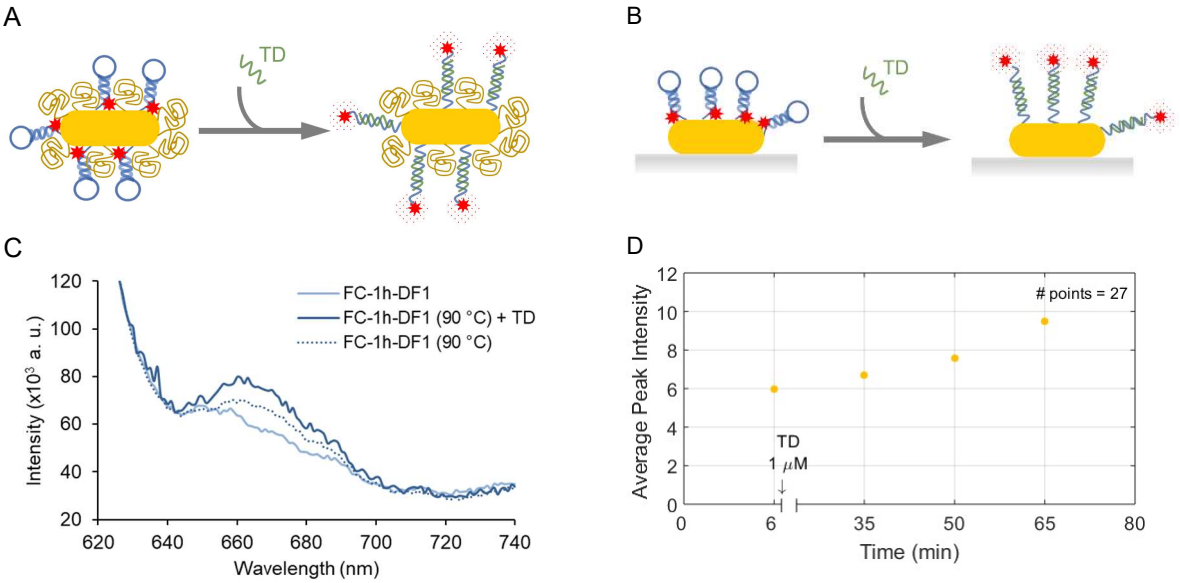

Figure 8: A - Schematic for FC-1h-DF1 response to TD in solution. B – Schematic for inSituDF1 response to TD. C - Emission spectra of FC-1h-DF1 in PBST. Response of starting solution (FC-1h-DF1) to TD target (FC-1h-DF1 (90º C) + TD) in saturation condition. Control solution (FC-1h-DF1 (90 ºC)) heated to 90 º C. D – Average peak intensity in relation to time of inSituDF1 prior and after introduction of 2 µL of TD target (100 µM) in ca. 20 µL PBS 1x (coverslip with tank). '# points' indicates the number of points analysed.

CONCLUSIONS AND FUTURE OUTLOOK

In this work, single particle fluorescence spectroscopy of DNA-AuNRs with ATTO647N was performed. The acquired data agreed with theoretical simulations and ensemble spectroscopy measurements done at the host laboratory. Furthermore, the results denoted that the chosen immobilization methods might induce sample aggregation and significantly alter photophysical characteristics compared to the colloidal sample. From a single-particle discriminated analysis, particle-to-particle variability could be accounted for and correlation of different optical variables illustrated the in-sample heterogeneity.

Two approaches for DNA conjugation onto AuNRs were assessed: FC and Tip-selective functionalized nanohybrids. Between FC and Tip samples, the later emerge as structures with great potential for nanobiosensors, since in Tip-specific functionalization a low number of dyes generates signals of the same order of magnitude as heavily loaded AuNRs from FC functionalization protocol. Transposing this logic for AuNR loaded with molecular beacons, this would imply a lower limit of detection (higher sensitivity) for tip-selective nanohybrids over non-selectively functionalized ones.

Also in this work, fluorescence signalling of the molecular beacons in the absence of AuNRs was assessed in terms of quantum yield and lifetime, which advocated that the current molecular beacon design with a quencher labelled probe loop is unsuitable, under the conditions studied, for building sensitive AuNR based nanobiosensors.

Furthermore, fluorescence signalling in AuNRs-DF1 nanohybrids was tested yielding inconclusive target response. However, some steps can be taken to improve both explored systems: FC-DF1 – increased DF1 loading per AuNR, tweaking of salt concentration and determining a reasonable temperature and time range for easing target hybridization; InSituDF1 – equipment optimization (e.g. oil immersion objective lens), redesign of AuNR-dye pairing (bigger AuNRs scatter more light and ATTO680 would be closer to the centre of the current band pass filter at 695 nm).

On the whole, even though this research is at an onset stage, it can undoubtedly progress towards a highly sensitive sensor for the enhanced optical detection of target oligonucleotides, that could eventually be used for cell imaging or in a microfluidic device for a lab-on-a-chip application.

ACKNOWLEDGEMENT

This document was written and made publicly available as an institutional academic requirement and as a part of the evaluation of the MSc thesis in Biomedical Engineering of the author at Instituto Superior Técnico. The work described was performed at the *Centro de Química Estrutural* of *Instituto Superior Técnico (Lisbon, Portugal),* during the period March-July 2019, under the supervision of Prof. Pedro Paulo.

REFERENCES

[1] V. Giannini, A. I. Fernández-Domínguez, S. C. Heck, and S. A. Maier, "Plasmonic Nanoantennas: Fundamentals and Their Use in Controlling the Radiative Properties of Nanoemitters," *Chem. Rev.*, vol. 111, no. 6, pp. 3888–3912, 2011.

[2] D. Botequim, I. I. R. Silva, S. G. Serra, E. P. Melo, and D. M. F. Prazeres, "Fluorescent Dye Nano-Assemblies by Thiol Attachment Directed to the Tips of Gold Nanorods for an Effective Plasmon-Enhanced Emission." (ready for submission)

[3] P. M. R. Paulo and S. M. B. Costa, "Single-molecule fluorescence of a phthalocyanine in pamam dendrimers reveals intensity-lifetime fluctuations from quenching dynamics," *J. Phys. Chem. C*, vol. 114, no. 44, pp. 19035–19043, 2010.

[4] C. Würth, M. Grabolle, J. Pauli, M. Spieles, and U. Resch-Genger, "Relative and absolute determination of fluorescence quantum yields of transparent samples," *Nat. Protoc.*, vol. 8, no. 8, pp. 1535–1550, 2013.

[5] A. M. Brouwer, "Standards for photoluminescence quantum yield measurements in solution (IUPAC Technical Report)," *Pure Appl. Chem.*, vol. 83, no. 12, pp. 2213–2228, 2011.

[6] Image Analyst, "Image Segmentation Tutorial - File Exchange - MATLAB Central," *MATLAB Central File Exchange*, 2008. [Online]. Available: https://nl.mathworks.com/matlabcentral/fileexchange/25157-image-segmentation-tutorial. [Accessed: 18-Mar-2019].

[7] S. Stein, "Fast Gaussian Point Spread Function Fitting (MEX) – File Exchange – MATLAB Central." [Online]. Available: https://www.mathworks.com/matlabcentral/fileexchange/52417-fast-gaussian-point-spread-function-fitting-mex. [Accessed: 19-Mar-2019].

[8] P. Zijlstra and M. Orrit, "Single metal nanoparticles: Optical detection, spectroscopy and applications," *Reports Prog. Phys.*, vol. 74, no. 10, 2011.

[9] M. Yorulmaz, S. Khatua, P. Zijlstra, A. Gaiduk, and M. Orrit, "Luminescence quantum yield of single gold nanorods," *Nano Lett.*, vol. 12, no. 8, pp. 4385–4391, 2012.

[10] J. W. Ha, "Chemical interface damping of single gold nanorods with low sensitivity to the medium dielectric constant," *Chem. Phys. Lett.*, vol. 676, pp. 65–69, 2017.

[11] N. Xu, B. Bai, Q. Tan, and G. Jin, "Fast statistical measurement of aspect ratio distribution of gold nanorod ensembles by optical extinction spectroscopy," *Opt. Express*, vol. 21, no. 3, p. 2987, 2013.

[12] V. Amendola, R. Pilot, M. Frasconi, O. M. Maragò, and M. A. Iatì, "Surface plasmon resonance in gold nanoparticles: A review," *J. Phys. Condens. Matter*, vol. 29, no. 20, 2017.

[13] P. Zijlstra, P. M. R. Paulo, K. Yu, Q. H. Xu, and M. Orrit, "Chemical interface damping in single gold nanorods and its near elimination by tip-specific functionalization," *Angew. Chemie - Int. Ed.*, vol. 51, no. 33, pp. 8352–8355, 2012.

[14] N. D. Burrows *et al.*, "Surface Chemistry of Gold Nanorods," *Langmuir*, vol. 32, no. 39, pp. 9905–9921, 2016.

[15] K. L. Blythe and K. A. Willets, "Super-Resolution Imaging of Fluorophore-Labeled DNA Bound to Gold Nanoparticles: A Single-Molecule, Single-Particle Approach," *J. Phys. Chem. C*, vol. 120, no. 2, pp. 803–815, 2016.

[16] "ATTO-TEC Fluorescent Labels and Dyes." [Online]. Available: https://www.atto-tec.com/attotecshop/product_info.php?language=en&info=p114_atto-647n.html&. [Accessed: 15-Jan-2019].

[17] R. Tsukanov *et al.*, "Detailed study of DNA hairpin dynamics using single-molecule fluorescence assisted by DNA origami," *J. Phys. Chem. B*, vol. 117, no. 40, pp. 11932–11942, 2013.